Local electronic structures of ZnSe/Si nanotapes and their luminescence properties

Quan Li, S. K. Hark, Juan Wang, Y. M. Xu, C. R. Wang, and W. M. Lau
Department of Physics, The Chinese University of Hong Kong, Shatin, New Territory, Hong Kong

(Received 14 June 2005; accepted 22 September 2005; published online 18 November 2005)

ZnSe/Si nanotapes have been fabricated via a co-assisted vapor-phase transfer mechanism. Local electronic structure investigation along the nanotape radial direction suggests that the Si surface can be terminated by the ZnSe, leading to the one-dimensional (1D) anisotropic growth of Si, and further results in direct interface between ZnSe and Si in the nanotapes. The co-growth mechanism not only results in nanowire heterostructures, but also effectively incorporates Si into ZnSe and thus modifies its luminescence properties, leading to luminescence peak both above and below the original band gap of pure phase ZnSe. © *2005 American Institute of Physics*.
[DOI: 10.1063/1.2133891]

ZnSe (bulk crystal E_g=2.7 eV at 300 K) (Ref. 1) is one of the key materials for applications in short-wavelength optoelectronics devices.[2–4] ZnSe-based microstructures have been widely investigated in recent years for their potential optoelectronic applications in high-density optical storage, full-color display, etc.[5–7] Moreover, ZnSe exhibits a significantly larger exciton binding energy [21 meV (Ref. 8)] in comparison to that of GaAs [4.2 meV (Ref. 9)], which makes it an ideal candidate for efficient room temperature exciton devices and devices with improved temperature characteristics.[1]

In recent years, its one-dimensional nanostructures have aroused much research interest due to their potential to serve as ideal building blocks for nanoscale optoelectronics in the bottom-up approach.[10–12] Nevertheless, real device application would require both heterojunction formation in the 1D nanostructures and effective doping of them. Despite the fact that phase pure single crystalline ZnSe nanowires with high electronic structure quality have been successfully synthesized using various physical/chemical methods,[13–15] limited work has been devoted to either the heterojunction formation or doping of such nanowires.[16]

In this study, we demonstrate the synthesis of ZnSe/Si nanotapes based on a co-assisted growth mechanism, i.e., the ZnSe confines the one-dimensional growth of the Si, while the Si serves as the template for the ZnSe growth. The microstructure, local electronic structure and the luminescence properties of the nanotapes are investigated. We found the co-growth mechanism not only results in nanowire heterostructures, but also effectively dopes Si into ZnSe and thus modified its luminescence properties.

The nanostructures were grown using a high-temperature vacuum tube furnace, whose settings can be found elsewhere.[17] ZnSe powder and Si/SiO_2 (50 wt. %) powder mixtures were placed separately on two alumina boats in the center region of the alumina tube, and quartz substrates were placed in the downstream of the tube. The tube was then pumped down to a base pressure of 2×10^{-2} Torr. Ar -5 % H_2 was introduced into the tube at a constant flow rate of 50 sccm. The total pressure was maintained at 300 Torr during the fabrication process. The furnace was maintained at 1300 °C for 2 h before it was cooled down to room temperature. The general morphology and crystallinity of the sample was examined by scanning electron microscopy (SEM, LEO 1450VP), and x-ray diffraction (XRD, Rigakau RU-300 with Cu $K\alpha$ radiation), respectively. Detailed microstructure analysis was conducted using a scanning transmission electron microscope (Tecnai 20, 200 kV, FEG). The dark field image was taken using the high angle annular dark field detector. The local electronic structure of the nanowire was investigated by spatially-resolved valence electron energy loss spectroscopy (VEELS) performed in a line scan mode using the Gatan Imaging filtering (GIF) system attached to the same microscope. The electron probe size was $\simeq$1 nm. The VEELS spectra were taken at small momentum transfer with an energy resolution of 0.7 eV and angular resolution of 0.2 mrad. The corresponding loss functions were deducted using the conventional Fourier-Log algorithm. The PL spectra were measured from the sample mounted on a cold finger in a continuous cycle cryostat using the 325 nm line of a HeCd laser. Both the as-synthesized and HF-dipped nanotape samples were examined.

The as-synthesized products demonstrate wire-like morphology from the SEM inspections. All of the diffraction peaks in the XRD can be indexed to those of standard Si, hexagonal and cubic ZnSe within the experimental error. No obvious peak shifting is detected. The detailed morphology/microstructure of the nanowire is revealed by the TEM. The low magnification bright field TEM image shown in Fig. 1(a) shows a typical single nanowire with dark/light contrast running side by side along the wire growth direction, demonstrating the nanotape configuration. Such a configuration is further supported by the image taken from the XTEM sample, in which the side-by-side feature can be clearly seen [inset of Fig. 1(a)]. The chemical composition of the nanotape and the spatial distribution of the compositional elements are illustrated by the corresponding EELS mapping of the same nanotape shown in Fig. 1(a). By overlapping the three elemental maps of Zn, Se, and Si with the original bright field image, one can find good correlations between Zn, Se and the dark contrast, and Si and the light contrast, respectively. No oxygen signal is detected within the detection limit of the spectrometer. While the Si phase is cubic, both hexagonal and cubic ZnSe exist in the nanotapes. The surfaces of both ZnSe and Si are smooth, as demonstrated in Figs. 1(e) and 1(f), respectively. Although the interface be-

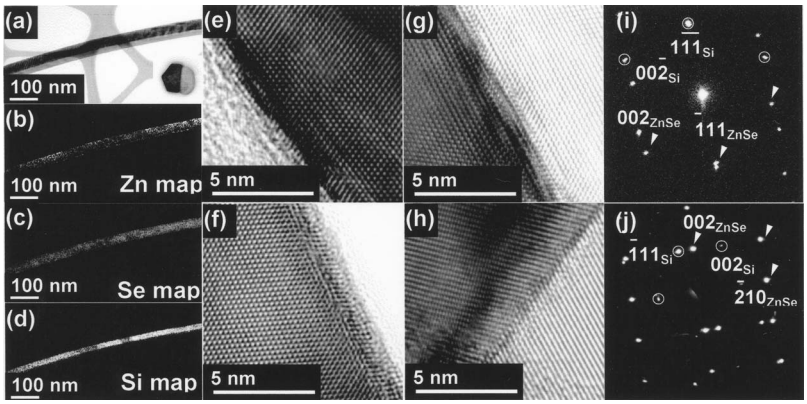

FIG. 1. (a) Low magnification TEM image of single nanotape. The inset of (a) shows a typical cross section of such nanotape; (b), (c), (d) The corresponding elemental map of the nanotape shown in (a), using the Zn *L* edge at 1020 eV, Se *M* edge at 1435 eV, and Si *K* edge at 1839 eV, respectively; (e) High resolution image showing the termination surface of ZnSe; (f) High resolution image showing the termination surface of Si; (g) High resolution image of cubic-ZnSe/Si interface; (h) High resolution image of hexagonal-ZnSi interface; (i) Diffraction pattern taken from the cubic-ZnSe/Si interface; (j) Diffraction pattern taken from the hexagonal-ZnSe/Si interface.

tween the ZnSe and the Si is sharp locally [Figs. 1(g) and 1(h)], it is usually not perfect—stacking faults are constantly observed. Good epitaxial relationship is always achieved in-between the cubic ZnSe and the Si {usually in a twin format, which is indicated by both the high resolution image [Fig. 1(g)] and the diffraction pattern [Fig. 1(i)] taken from the cubic-ZnSe/Si interface}. Nevertheless, no specific orientation relation is detected when the ZnSe phase is hexagonal, as suggested by both the high resolution image [Fig. 1(h)] and the diffraction pattern [Fig. 1(j)] taken from the hexagonal-ZnSe/Si interface.

The local electronic structure of such nanotape is examined using valence electron energy loss spectroscopy (VEELS). The inset of Fig. 2(a) shows the dark field image of a small portion of the nanotape, in which the white contrast corresponds to ZnSe and the grey contrast to Si. The VEELS was performed in a line scan mode starting from the inner ZnSe to the Si edge, as represented by the line mark in the dark field image. The total scanning length is 30 nm, with 40 steps taken in between. The corresponding loss functions are plotted in Fig. 2(a) with some of the data omitted (those taken from the inner part of the ZnSe as well as the Si are basically repeating the main features of each individual). The negative secondary differentiations of the loss functions are shown in Fig. 2(b), so that the peak features in the loss functions are manifested for easy observations. All of the peak features, including the interband transitions at 7.6 eV and 20.5 eV, the *D* band transition at 14.8 eV, the surface state-related transition at 11.7 eV, and the bulk plasmon loss at 17.7 eV, in the loss function (plot 1) taken from the inner part of ZnSe resemble those of the bulk ZnSe.[18] Starting from plot 2 to plot 5, the loss functions gradually change from that of bulk ZnSe to Si until plot 6, in which the loss function feature becomes characteristic of bulk Si with only a sharp plasmon loss at 16.8 eV. Not only the peak features corresponding to all of the ZnSe interband transitions are gradually weakened, its bulk plasmon peak also redshifts. By correlating the loss function data with the original dark field image, one can find good correlation between the transitions in the spectra and the ZnSe/Si interfacial region, which lasts $\simeq$3 nm as indicated by the corresponding loss functions. It is interesting to note that the bulk Si feature does not last to the termination surface of the Si side (plot 9–10), where peaks features corresponding to the ZnSe interband transition (7.6 eV) reappears, and the plasmon oscillation also blue shifts to that of bulk ZnSe. Additional feature also appear in the position of the original surface state-related transition of ZnSe (11.7 eV), but with different line shapes. Such surface region lasts $\sim$1–2 nm.

The experimental facts suggest that these ZnSe/Si bicrystalline based nanostructures are grown via a co-growth vapor transfer mechanism—ZnSe and Si simultaneously presents in the vapor phase, which is transferred to the lower temperature zone and condenses together to form the specific nanotape configuration. The 1D growth of Si in the nanotape is governed by a physical principle similar to the oxide-assisted growth (OAG) mechanism.[19,20] Nevertheless, unlike the oxide-assisted SiNW growth, it is not the O, which terminates specific surfaces of Si and decides the specific an-

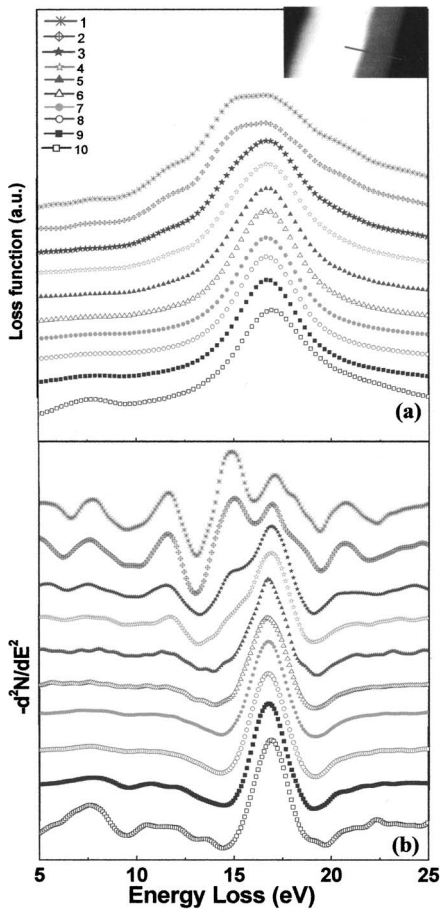

FIG. 2. (a) The loss functions of the nanotape obtained from the VEELS spectra taken in a line scan mode across the nanotape interface. The scan line is shown in the dark field image of a small portion of the nanotape in the inset of (a). (b) The corresponding negative secondary differentiation of the loss functions shown in (a).

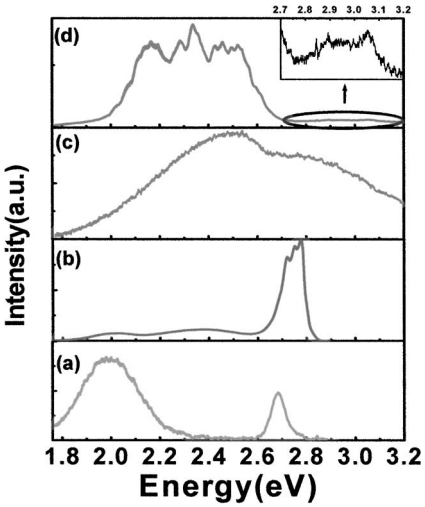

FIG. 3. (a), (b) Room temperature and 10 K photoluminescence spectra taken from phase pure ZnSe nanowires [with typical morphology shown in the inset of (a)]; (c), (d) Room temperature and 10 K photoluminescence spectra taken from the nanotapes.

isotropic SiNW growth. Instead, the ZnSe in the vapor phase plays an important role. This is supported by the VEELS results shown in Fig. 2, in which the electronic structure of the Si surface region indicate the presence of ZnSe. Nevertheless, such ZnSe appears to be different from its bulk form, as not all the characteristic features of the loss function have been repeated. In fact, the surface-related weak oscillations at ~12 eV suggest possible intermixing of Si and ZnSe, which has changed the chemical state and thus the electronic structure of the ZnSe in the Si surface region.[18] Once terminated the specific surfaces of Si [(111) planes in this case], the ZnSe serves as preferential sites for the homophase nucleation, resulting in ZnSe/Si nanotapes.

Figure 3 shows the PL spectra of ZnSe/Si nanotapes at room temperature and at 10 K. Also shown in the figure are spectra of phase pure ZnSe nanowires at the same temperatures for comparison. We note that the optical property of the latter is good, displaying a near-band-edge emission (NBE) peak (~2.7 eV) even at room temperature [Fig. 3(a)]. A broad deep level emission band (DLE) centered around 2.0 eV is also found. At 10 K, the NBE peak blueshifts to 2.78 eV, greatly intensifies relative to the DLE and sharpens to allow its phonon replicas be clearly resolved [Fig. 3(b)]. Pure phase Si nanowires of similar size (~20–30 nm in diameter) do not give any luminescence peaks. Had there be complete absence of reaction between or mixing of Si and ZnSe during their simultaneous growth, one would expect the PL spectra of ZnSe/Si nanotapes be similar to that of the ZnSe nanowires. Experimentally, we find that their measured room temperature and 10 K spectra are distinctly different [Fig. 3(c)]. More importantly, emissions at energies much higher than the band gap of ZnSe are found. We may rule out SiO_x and porous silicon as the sources that give rise to the peculiar spectra, since dipping of the nanotapes into HF, intended to remove possible oxides and hydroxides of silicon, did not lead to any significant changes in the measured spectra. The PL spectra suggest to us that Si–ZnSe reaction products, at concentrations too low to be detected except by PL in our experiments, have interdispersed into the bi-crystalline nanotapes. Some support of this suggestion comes from the VEEL spectra 9–11 of Fig. 2 that identified ZnSe-like plasmon at the outer edge of the Si part of the nanotapes. Intermixing or reaction of ZnSe with Si has also been suggested in the MBE growth of ZnSe epilayers on Si substrates[21] and in Si–ZnSe biaxial nanowires.[16] Some of the reaction products are responsible for the above ZnSe band gap emissions and others for the below band gap emissions. We note that the broad below band gap emissions develop certain sharp features at 10 K [Fig. 3(d)], suggesting Si might act as at a radiative recombination center in ZnSe.

Although both the crystalline structure (as suggested by XRD and TEM) and the overall electronic structure (as suggested by the VEELS) of the ZnSe and the Si remain the same as their phase pure bulk counterparts, chemical mixing occurs at both the interfacial region and the Si surface region. The PL results suggest that the Si has been introduced in the ZnSe, and thus significantly affect its luminescence properties. In general, the II-VI 1D nanostructures are promising building blocks for nanophotonic applications. Nevertheless, real device application usually requires heterojunction formation and effective doping of them. The current work provides an effective approach addressing the above two issues, which contributes to the realization of the next generation of functional nanodevices utilizing these 1D nanostructures.

The work was fully supported by a grant from the Research Grant Council of HKSAR under Project No. CUHK 400904.

[1] R. Rujkorakarn and Art J. Nelson, J. Appl. Phys. **87**, 8557 (2000).
[2] T. Matasuoka, Adv. Mater. (Weinheim, Ger.) **8**, 469 (1996).
[3] R. Pässler, E. Griebl, H. Ripel, G. Lautner, S. Bauer, H. Preis, W. Gebhardt, B. Buda, D. J. As, D. Schikora, K. Lischka, K. Papagelis, and S. Ves, J. Appl. Phys. **86**, 4403 (1999).
[4] J. Wang, D. C. Hutchings, A. Miller, E. W. Vanstryland, K. R. Welford, I. T. Muirhead, and K. L. Lewis, J. Appl. Phys. **73**, 4746 (1993).
[5] S. K. Hong, E. Kurts, J. H. Chang, T. Hanada, M. Oku, and T. Yao, Appl. Phys. Lett. **78**, 165 (2001).
[6] M. A. Haase, J. Qiu, J. M. Depuydt, and H. Cheng, Appl. Phys. Lett. **59**, 1272 (1991).
[7] H. Jeon, J. Ding, W. Patterson, A. V. Nurmikko, W. Xie, D. C. Grillo, M. Kobayashi, and R. L. Gunshor, Appl. Phys. Lett. **59**, 3619 (1991).
[8] Z. M. Zhu, N. Z. Liu, G. H. Li, H. X. Han, Z. P. Wang, S. Z. Wang, L. He, R. B. Ji, and Y. Wu, J. Infrared Millim. Waves **18**, 13 (1999).
[9] S. Z. Wang, S. F. Yoon, L. He, and X. C. Shen, J. Appl. Phys. **90**, 2314 (2001), and references therein.
[10] X. F. Duan, Y. Huang, R. Agarwal, and C. M. Lieber, Nature (London) **421**, 241 (2003).
[11] X. F. Duan, C. M. Niu, V. Sahi, J. Chen, J. W. Parce, S. Empedocles, and J. L. Goldman, Nature (London) **425**, 274 (2003).
[12] Y. Huang, X. F. Duan, Y. Cui, L. J. Lauhon, K. H. Kim, and C. M. Lieber, Science **294**, 1313 (2001).
[13] Q. Li, X. G. Gong, C. R. Wang, J. Wang, K. Ip, and S. K. Hark, Adv. Mater. (Weinheim, Ger.) **16**, 1436 (2004).
[14] X. T. Zhang, K. M. Ip, Z. Liu, Y. P. Leung, Q. Li, and S. K. Hark, Appl. Phys. Lett. **84**, 2641 (2004).
[15] Y. C. Zhu and Y. Bando, Chem. Phys. Lett. **377**, 367 (2003).
[16] J. Hu, Y. Bando, Z. Liu, T. Sekiguchi, D. Golderg, and J. Zhan, J. Am. Chem. Soc. **125**, 11306 (2003).
[17] Q. Li and C. R. Wang, Appl. Phys. Lett. **82**, 1398 (2003).
[18] R. L. Hengehold and F. L. Pedrotti, Phys. Rev. B **6**, 3026 (1972).
[19] N. Wang, Y. F. Zhang, Y. H. Tang, C. S. Lee, and S. T. Lee, Appl. Phys. Lett. **73**, 3902 (1998).
[20] N. Wang, Y. F. Zhang, Y. H. Tang, C. S. Lee, and S. T. Lee, Phys. Rev. B **58**, R16024 (1998).
[21] R. D. Bringans and M. A. Olmstead, Phys. Rev. B **39**, 12985 (1989); R. D. Bringans, D. K. Biegelsen, L.-E. Swartz, F. A. Ponce, and J. C. Tramontana, *ibid.* **45**, 13400 (1992).